---

**Article:**
Liu, Z., Liu, Y. and Chu, X. orcid.org/0000-0003-1863-6149 (2024) Reconfigurable intelligent surface-assisted indoor millimeter-wave communications for mobile robots. IEEE Internet of Things Journal, 11 (1). pp. 1548-1557. ISSN 2327-4662

https://doi.org/10.1109/JIOT.2023.3289772

---

# Reconfigurable Intelligent Surface-assisted Indoor Millimeter-wave Communications for Mobile Robots

Zhiyu Liu, Yang Liu, *Member, IEEE*, and Xiaoli Chu, *Senior Member, IEEE*

***Abstract*—Reconfigurable intelligent surfaces (RISs) and millimeter-wave (mmWave) communications have been considered for providing wireless connectivity to mobile robots used in industrial plants and other indoor environments. However, the existing works have not sufficiently studied how the number and deployment locations of RISs should be optimized for serving a mobile robot. In this paper, we study RIS-assisted mmWave communications for a robot moving around fixed obstacles in an indoor industrial environment. For a fixed total number of reflecting elements, we formulate an optimization problem to minimize the transmission energy consumption of the access point (AP) while ensuring the robot's received signal-to-noise ratio (SNR) above a threshold throughout its journey by jointly optimizing the number, positions and phase shifts of RISs and the beamforming vectors of the AP. To solve the formulated non-convex optimization problem, we devise an iterative algorithm that decomposes it into two subproblems (i.e., optimizing the phase shifts of RISs and the beamforming vector of the AP, and optimizing the number and locations of RISs) and solves them alternately. Simulation results show that the proposed algorithm converges fast and can obtain the best number and locations of RISs that lead to a transmission energy consumption of the AP much lower than the benchmark schemes.**

***Index Terms*—Reconfigurable intelligent surface deployment, millimeter-wave, mobile robot, energy consumption, beamforming.**

## I. Introduction

As the industrial Internet of things (IIoT) continues to expand, wirelessly connected mobile robots are expected to be in increasingly widespread use, carrying out various tasks [1]. Due to the presence of machines, furniture and other things in an industrial environment, the line-of-sight (LoS) link between an access point (AP) and a mobile robot is likely to be blocked while the robot is moving around them. This makes it difficult to employ millimeter-wave (mmWave) communications for mobile robots because non-line-of-sight (NLoS) mmWave links suffer from severe penetration losses [2], [3].

To increase the possibility of a receiver seeing a LoS link and to enable continuous connectivity, reconfigurable intelligent surfaces (RISs) have been employed to reflect signals from a transmitter to a receiver [4]. An RIS is a planar surface composed of reconfigurable passive reflecting elements, each being capable of controlling the amplitude and phase shift of their reflected signal [5], and has attracted a lot of interest from researchers. In [6], the authors minimized the transmit power of the AP by jointly optimizing the phase shifts of elements on a single RIS and the beamforming vectors at the AP while meeting the downlink signal-to-interference-plus-noise ratio (SINR) requirement. Their results demonstrated that the transmit power at the AP can be scaled down by $1/N^2$, where $N$ denotes the number of elements on the RIS. In [7], the authors maximized the downlink received signal-to-noise ratio (SNR) in a single RIS-aided multiple-input single-output (MISO) mmWave communication system by optimizing the phase shifts of the RIS and found that the RIS achieved a lower outage probability than amplify-and-forward (AF) relaying. In [8], the authors maximized the downlink received signal power in a RIS-aided MISO system by jointly optimizing the active beamforming at the AP and passive beamforming at the RIS. We note that only a single RIS was considered in [6]–[8] and their results cannot be readily extended to cases of multiple RISs.

Depoying multiple RISs opens the door to more design variables, such as the number and deployment positions of RISs. In [9], the simulation results showed that a distributed deployment of multiple RISs across the service area of a base station (BS) can improve the mean rate of all the users as compared with the full-duplex (FD) relaying; and when centralizing the fixed total number of elements on fewer RISs, the mean user rate will increase but the fairness among spatially distributed users in terms of their achievable rates will degrade. In [10], the authors found that for a fixed total number of elements, deploying one RIS achieves a larger capacity region for two single-antenna users of different data rate requirements than deploying two RISs. In [11], the results showed that deploying two RISs can increase the downlink received signal power by a factor of $\mathcal{O}(N^4)$, while that of deploying a single RIS is $\mathcal{O}(N^2)$, where $N$ is the total number of reflecting elements. In [12], the authors showed that with a fixed total number of elements, the distributed deployment of multiple RISs (at the same height on a vertical 2D plane) can achieve a higher downlink ergodic capacity than deploying a single RIS under outdated channel state information in a single-input single-output (SISO) system. In [13], the authors maximized the downlink sum rate of all users in a multi-RIS-aided MISO system by jointly optimizing the beamforming

This work was supported in part by the European Union's Horizon 2020 Research and Innovation Program under the Marie Skłodowska-Curie Actions with Grant Agreement No. 778305. *(Corresponding author: Xiaoli Chu.)*

Zhiyu Liu, Yang Liu, and Xiaoli Chu are with the Electronic and Electrical Engineering Department, The University of Sheffield, Sheffield S1 4ET, UK (e-mail: zliu160@sheffield.ac.uk; liuyang91e@gmail.com; x.chu@sheffield.ac.uk).

vector at the BS, the phase shifts at the RISs and the block-length for ultra-reliable low-latency communication (URLLC) subject to a maximum allowed packet error probability. In [14], the authors jointly optimized the locations of UAVs each carrying an RIS, the phase shifts of the RISs and the BS transmit power to minimize the number of RISs required for meeting a downlink received SNR requirement. However, the above studies on the deployment of multiple RISs all assumed that the user devices were stationary. Their results cannot be readily extended to the cases of moving users, because the LoS/NLoS status of the links from the RISs and BSs to the users may change as the users move around obstacles. Moreover, in [10]-[12], only two RISs were considered, while the locations of them were not optimized.

Recently, RIS-assisted communications for moving objects have been studied. In [15], the authors maximized the uplink average data rate of a robot moving from an initial position to a target position within a limited time by jointly optimizing the phase shifts of an RIS deployed nearby, the trajectory and the beamforming vector of the robot. In [16], the trajectory and speed of a UAV (carrying a RIS) and the phase shifts of the RIS were jointly optimized to maximize the average downlink rate of a vehicle that moves along a road in an urban area. In [17], the authors analyzed the coverage probability of a single-antenna vehicle served by a UAV carried BS and a single RIS deployed on the exterior wall of a building while the vehicle drives along a straight motorway for different positions of the UAV. In [18], for a vehicular network assisted by a UAV carried RIS, the authors maximized the minimum downlink throughput among all the vehicles served by a BS by jointly optimizing the phase shifts of the RIS, transmission scheduling, transmission power of the BS and the UAV trajectory. In [15]-[18], only a single RIS was considered. In [19], the vehicles moving along a straight motorway were served by a BS carried by a UAV and multiple RISs deployed on a vertical 2D plane that is parallel to motorway, where each RIS served a different vehicle. The authors minimized the sum outage probability of all the vehicles by optimizing the transmit power of the BS, but the locations or number of RISs were not optimized. We note that in the above works, the LoS/NLoS status of each link was statistically characterized by an independent LoS probability, but the impact of blockage(s) on the wireless links seen by a moving user was not explicitly modeled.

In this paper, we study RIS-assisted mmWave communications for a mobile robot in an indoor industrial environment with large obstacles. Aiming to minimize the transmission energy consumption of the AP, we investigate whether a fixed number of passive elements should be distributed to a large number of small RISs or centralized to a small number of large RISs, while maintaining reliable downlink communications for a robot moving around the obstacles along a known trajectory within a given time limit. The contributions of this paper are summarized as follows:

- We present a system model for the RIS-assisted mmWave downlink transmission from an AP on the ceiling to a robot moving around obstacles at fixed locations inside an industrial plant, where one or multiple RISs are deployed on a selected wall. At each position along its trajectory, whether the robot sees a LoS or NLoS link from an RIS or the AP is explicitly modelled for the considered indoor industrial environment. This is different from the existing works [15]-[19] where the effects of blockages on the links from the RISs or APs to the moving users (e.g., vehicles or robots) were not explicitly modeled.
- We formulate an optimization problem to minimize the transmission energy consumption of the AP while guaranteeing that the received SNR at the robot is kept above a threshold throughout its journey by jointly optimizing the number, positions and phase shifts of RISs and the beamforming vectors of the AP. The difficulties of this optimization problem mainly lie in the unfixed number of variables that are coupled in both the objective function and the constraint on the received SNR in complicated ways. This is different from the existing works where only a single RIS was considered [6]-[8], [15]-[18], the locations or numbers of RISs were not optimized [10]-[12], [19], or users were assumed to be stationary [6]-[14].
- Since the formulated joint optimization problem is non-convex and difficult to solve directly, we decompose it into two subproblems and solve them alternately. More specifically, for given number and locations of RISs, we devise a Total Energy Consumption Optimization (TECO) Algorithm to minimize the AP's transmission energy consumption by iteratively optimizing the phase shifts of each RIS and the beamforming vector of the AP. For given phase shifts of the RISs and beamforming vectors of the AP, we devise a genetic algorithm to find the optimal number and deployment locations of RISs that minimize the AP's transmission energy consumption. Then, we propose a RIS Locations and Number (RISLN) Algorithm that iteratively calls the TECO Algorithm and the genetic algorithm until the decrease of the AP transmission energy consumption is below a threshold.
- Our simulation results demonstrate that the proposed algorithms converge fast and can find the suitable number and best deployment locations of RISs that minimize the AP's transmission energy consumption while maintaining reliable communications between the AP and the robot. The simulation results also show that the transmission energy consumption of the AP decreases when the fixed total number of reflecting elements are shared by more distributed RISs, but the reduction in AP transmission energy consumption stops when the number of RISs becomes too large.

The rest of the paper is organized as follow. In Section II, we introduce the system model, LoS/NLoS status indicator vector and channel model. In Section III, we formulate the AP's transmission energy consumption minimization problem and propose algorithms to solve it. In Section IV, we provide

simulation results. Finally, we conclude the paper in Section V.

## II. System Model

### A. System Model

As shown in Fig. 1, we consider an industrial indoor environment containing several parallel rows of interior obstacles (e.g., large machines or shelves deployed in parallel across the industrial plant) in a Cartesian coordinate system, where one of the ground corners of the plant is set as the origin of the horizontal plane. The plant has a rectangular floor area of $l_f \times l_p$, where $l_f$ is the length of the wall perpendicular to the rows of obstacles, and $l_p$ is the length of the wall parallel to the rows of obstacles. We model the parallel obstacles as evenly spaced identical convex cubes each of length $L$, width $W$, and height $H$, where the distance between any two adjacent obstacle is $l_a$, and the number of obstacles is given by $I \leqslant l_f/(l_a+W)$. A robot moves on the horizontal ground plane around the parallel rows of obstacles from a starting point $q_s$ to a destination point $q_d$ along a fixed trajectory (as indicated by the dashed line on the ground plane in Fig. 1). The trajectory keeps a distance of $l$ ($< l_a/2$) meters from the closet obstacle and forms a U shaped route between any two adjacent obstacles. The obstacles locate along the robot's trajectory from $q_s$ to $q_d$ are denoted by $O_1, O_2, \cdots, O_I$, respectively. The corners of the obstacles closest to the start point are denoted by $q_{O_1}, q_{O_2}, \cdots, q_{O_I}$ and are used to represent the locations of the corresponding obstacles.

We consider the downlink from an access point (AP) mounted on the ceiling to the single-antenna robot. The AP is equipped with a uniform linear array (ULA) of $M$ ($>1$) antennas. The location of the AP is denoted by $q_A$. There are $K$ RISs deployed on a wall perpendicular to the obstacles to reflect signals from the AP to the robot. Each RIS is equipped with $\frac{N}{K}$ passive reflecting elements, where $N$ is the total number of passive reflecting elements of all the RISs. We assume that the reflecting elements on the RISs are all passive [5]-[7]. The deployment of RISs ensures the LoS links between the AP and themselves, and their locations are higher than the receive antenna on the robot. The locations of RISs are given by $\boldsymbol{q}_R = [q_{R_1}, q_{R_2}, \cdots, q_{R_K}]$, where $q_{R_k} = [x_{R_k}, y_{R_k}, z_{R_k}]$. The passive reflecting elements of each RIS form an uniform rectangular array (URA). For simplicity, the location of the central element of the AP's or an RIS's array is considered as the location of the AP or the RIS, which is used to calculate the distance between the AP or the RIS and another communication node [6]. Each RIS is connected to a smart controller that adjusts its phase shifts and reflection amplitudes via a separate wired link.

The time required for the robot to move from the start point to the destination along the fixed trajectory is divided into $T+1$ timeslots, $t = 0, \cdots, T$. Timeslot $t$ has a duration $\Delta_t$, which is sufficiently short so that the channel conditions can be assumed to be fixed within the timeslot. In timeslot $t$, the robot moves over a distance of $D_t = v_t\Delta_t$, where $v_t$ is the speed of the robot in timeslot $t$. We use the location of the robot antenna to represent the location of the robot at any time. The trajectory of the robot can be represented by $\boldsymbol{q} = [q_0, q_1, \cdots, q_T]$, where $q_t = [x_t, y_t, z_r]$ denotes the position of the robot in the $t$-th timeslot, $z_r$ is the height of the robot antenna above ground, $q_0 = q_s$, and $q_T = q_d$.

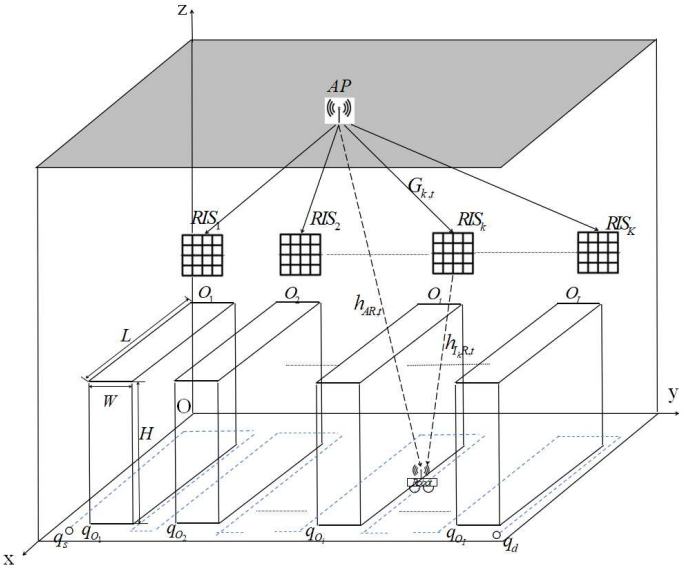


Fig. 1. System Model.

### B. LoS Indicator Matrix

The AP-robot and RIS$_k$-robot links ($k = 1, \cdots, K$) may become NLoS when they are blocked by obstacles as the robot moves along the trajectory. We define an $I \times (K+1)$ LoS indicator matrix at timeslot $t$:

$$\boldsymbol{\mu}^{(t)} = \begin{bmatrix} \mu_{10}^{(t)}, \mu_{11}^{(t)}, \cdots, \mu_{1K}^{(t)} \\ \mu_{20}^{(t)}, \mu_{21}^{(t)}, \cdots, \mu_{2K}^{(t)} \\ \vdots \quad \vdots \quad \vdots \\ \mu_{I0}^{(t)}, \mu_{I1}^{(t)}, \cdots, \mu_{IK}^{(t)} \end{bmatrix} \tag{1}$$

where $\mu_{i0}^{(t)} = 1$ if the LoS link between the AP and the robot is not blocked by the $i$-th obstacle at timeslot $t$, otherwise $\mu_{i0}^{(t)} = 0$; $\mu_{ik}^{(t)} = 1$ ($k = 1, \cdots, K$) if the LoS link between RIS$_k$ and the robot is not blocked by the $i$-th obstacle at timeslot $t$, otherwise $\mu_{ik}^{(t)} = 0$. We use a ray-slope method, as shown in Algorithm 1, to identify intersections between the $K+1$ links and the $I$ obstacles at timeslot $t$ [20], and obtain the LoS indicator matrix.

We note that the system model in Section II-A can be generalized by allowing each obstacle to have its distinct length, width and height, and by allowing different distances between different pairs of adjacent obstacles. In this way, the modeled obstacles can be of various sizes and do not necessarily locate along a straight line. The proposed Algorithm 1 can still obtain the LoS indicator matrix under such a more general setting of obstacles as long as the trajectory of the robot and the locations and sizes of the obstacles are pre-determined.

**Algorithm 1** LoS Indicator Vector

**Input:** $q_A$, $\boldsymbol{q}_R$, $\boldsymbol{q}_O$, $q_t$
**Output:** $\mu_{ik}^{(t)}(i=1,\cdots,I; k=0,1,\cdots,K)$

```
Initialize μ_ik^(t) = 0, (i = 1, ··· , I; k = 0, ··· , K)
for k = 0 to K do
    for i = 1 to I do
        Obtain the slope of the link between the AP and the robot/ the link between the k-th RIS and the robot with the input q_a, q_{R_k}, and q_t.
        Obtain the slope of the link between AP/RIS and the corner of the i-th obstacle with the input q_A, q_{R_k}, and q_{O_i}
        Obtain μ_ik^(t) by comparing the obtained slopes.
    end for
end for
```

### C. Channel Model

The channels from the AP to $RIS_k$, from the AP to the robot, and from $RIS_k$ to the robot at timeslot $t$ are denoted by $\boldsymbol{G}_k \in \mathbb{C}^{\frac{N}{K}\times M}$, $\boldsymbol{h}_{AR}^{(t)} \in \mathbb{C}^{1\times M}$, and $\boldsymbol{h}_{kR}^{(t)} \in \mathbb{C}^{\frac{N}{K}\times 1}$, respectively. Accordingly, $\boldsymbol{G}_k$ is given by [21]

$$\boldsymbol{G}_k = \sqrt{\rho d_{Ak}^{-2}} e^{-j2\pi\tau_{Ak}} \boldsymbol{c}_r(\mathcal{V}_{Ak}^{AoA}) \boldsymbol{c}_t(\mathcal{V}_{Ak}^{AoD}), \tag{2}$$

where $\rho$ ($<1$) denotes the LoS path loss at the reference distance of 1 m, $d_{Ak}$ denotes the distance between the AP and $\text{RIS}_k$, $\tau_{Ak}$ is the time of arrival (ToA) from the AP to $\text{RIS}_k$, $\boldsymbol{c}_r(\mathcal{V}_{Ak}^{AoA})$ and $\boldsymbol{c}_t(\mathcal{V}_{Ak}^{AoD})$ are respectively given by

$$\boldsymbol{c}_r(\mathcal{V}_{Ak}^{AoA}) = \left[1, \exp(\frac{j\pi d_A \sin\mathcal{V}_{Ak}^{AoA}}{\lambda_{AI}}), \cdots, \exp(\frac{j\pi d_A(\frac{N}{K}-1)\sin\mathcal{V}_{Ak}^{AoA}}{\lambda_{AI}})\right]^T, \tag{3}$$

$$\boldsymbol{c}_t(\mathcal{V}_{Ak}^{AoD}) = \left[1, \exp(\frac{j\pi d_A \sin\mathcal{V}_{Ak}^{AoD}}{\lambda_{AI}}), \cdots, \exp(\frac{j\pi d_A(M-1)\sin\mathcal{V}_{Ak}^{AoD}}{\lambda_{AI}})\right]^T, \tag{4}$$

where $\mathcal{V}_{Ak}^{AoA}$ and $\mathcal{V}_{Ak}^{AoD}$ are the angle of arrival (AoA) at $\text{RIS}_k$ from the AP and the angle of departure (AoD) at the AP towards $\text{RIS}_k$, respectively, $d_A$ is the spacing between any two adjacent antennas at the AP, and $\lambda_{AI}$ is the wavelength of the signal transmitted from the AP to $\text{RIS}_k$.

Similarly, $\boldsymbol{h}_{AR}^{(t)}$ is given by

$$h_{AR}^{(t)} = \begin{cases} \sqrt{\rho(d_{AR}^{(t)})^{-2}} e^{-j2\pi\tau_{AR}^{(t)}} \boldsymbol{c}_t(\mathcal{V}_{AR}^{AoD(t)}), & \mu_{i0}^{(t)} = 1, i = 1, \cdots, I \\ \sqrt{\rho(d_{AR}^{(t)})^{-\beta_{AR}}} e^{-j2\pi\tau_{AR}^{(t)}} \tilde{h}, & otherwise \end{cases}, \tag{5}$$

where $d_{AR}^{(t)}$ denotes the distance between the AP and the robot at timeslot $t$, $\beta_{AR}$ is the path loss exponent of the NLoS channel between the AP and the robot, $\tau_{AR}^{(t)}$ is the ToA from the AP to the robot at timeslot $t$, and $\tilde{\boldsymbol{h}} \sim \mathcal{CN}(0,1)$ is a $1 \times M$ vector whose elements follow independent complex Gaussian distribution with zero mean and unit variance, and $\boldsymbol{c}_t(\mathcal{V}_{AR}^{AoD(t)})$ is given by

$$\boldsymbol{c}_t(\mathcal{V}_{AR}^{AoD(t)}) = \left[1, \exp(\frac{j\pi d_A \sin\mathcal{V}_{AR}^{AoD(t)}}{\lambda_{AR}^{(t)}}), \cdots, \exp(\frac{j\pi d_A(M-1)\sin\mathcal{V}_{AR}^{AoD(t)}}{\lambda_{AR}^{(t)}})\right]^T, \tag{6}$$

where $\mathcal{V}_{AR}^{AoD(t)}$ is the AoD at the AP towards $\text{RIS}_k$ at timeslot $t$, and $\lambda_{AR}^{(t)}$ can be expressed as:

$$\lambda_{AR}^{(t)} = \frac{c}{f_c + \frac{f_c v_t \cos(\phi_{AR}^{(t)})}{c}}, \tag{7}$$

where $f_c$ is the carrier frequency of the AP transmission, $v_t$ is the velocity of the robot at timeslot $t$, $\phi_{AR}^{(t)}$ is the angle between the AP signal's AoA at the robot and the direction of the robot's motion, and $c$ is the speed of light.

Similarly, $\boldsymbol{h}_{kR}^{(t)}$ is given by

$$h_{kR}^{(t)} = \begin{cases} \sqrt{\rho(d_{kR}^{(t)})^{-2}} e^{-j2\pi\tau_{kR}^{(t)}} \boldsymbol{c}_t(\mathcal{V}_{kR}^{AoD}), & \mu_{ik}^{(t)} = 1, i = 1, \cdots, I \\ \sqrt{\rho(d_{kR}^{(t)})^{-\beta_{kR}}} e^{-j2\pi\tau_{kR}^{(t)}} \tilde{h}, & otherwise \end{cases}, \tag{8}$$

where $d_{kR}^{(t)}$ denotes the distance between $\text{RIS}_k$ and the robot at timeslot $t$, $\beta_{kR}$ is the path loss exponent of the NLoS channel between $\text{RIS}_k$ and the robot, $\tau_{kR}^{(t)}$ is the ToA from $\text{RIS}_k$ to the robot, and $\boldsymbol{c}_t(\mathcal{V}_{kR}^{AoD(t)})$ is given by

$$\boldsymbol{c}_t(\mathcal{V}_{kR}^{AoD(t)}) = \left[1, \exp(\frac{j\pi d_I \sin\mathcal{V}_{kR}^{AoD(t)}}{\lambda_{kR}^{(t)}}), \cdots, \exp(\frac{j\pi d_I(M-1)\sin\mathcal{V}_{kR}^{AoD(t)}}{\lambda_{kR}^{(t)}})\right]^T, \tag{9}$$

where $\mathcal{V}_{kR}^{AoD(t)}$ is the AoD at the AP at timeslot $t$, $d_I$ is the spacing between any two adjacent antennas at an RIS. $\lambda_{kR}^{(t)}$ is the wavelength of the siganl reflected by $\text{RIS}_k$ to the robot at timeslot $t$ and can be expressed as

$$\lambda_{kR}^{(t)} = \frac{c}{f_c + \frac{f_c v_t \cos(\phi_{kR}^{(t)})}{c}}, \tag{10}$$

where $\phi_{kR}^{(t)}$ is the angle between the AoA of the signal reflected by $\text{RIS}_k$ to the robot and the direction of the robot's motion.

The channel from the AP to the robot at timeslot $t$ is given by

$$\boldsymbol{h}^{(t)} = \sum_{k=1}^{K} (\boldsymbol{h}_{kR}^{(t)})^H \boldsymbol{\Theta}_k^{(t)} \boldsymbol{G}_k^{(t)} + \boldsymbol{h}_{AR}^{(t)}, \quad t = 0, \cdots, T, \tag{11}$$

where the diagonal matrix $\boldsymbol{\Theta}_k^{(t)} = diag(\eta_{k,1}^{(t)} e^{j\theta_{k,1}^{(t)}}, \cdots, \eta_{k,\frac{N}{K}}^{(t)} e^{j\theta_{k,\frac{N}{K}}^{(t)}})$ ($j$ denotes the imaginary unit) is the reflection-coefficients matrix of $\text{RIS}_k$ at timeslot $t$, $\theta_{k,n}^{(t)} \in [0, 2\pi)$ and $\eta_{k,n}^{(t)} \in [0,1]$ denote the phase shift and the reflection coefficient amplitude of the $n$-th element of the $k$-th RIS, respectively. For simplicity, we assume $\eta_{k,n}^{(t)} = 1, \forall n,k,t$, since the reflection coefficient amplitudes are typically set at their maximum value [6], and accordingly $\boldsymbol{\Theta}_k^{(t)} = diag(e^{j\theta_{k,1}^{(t)}}, \cdots, e^{j\theta_{k,\frac{N}{K}}^{(t)}})$.

We consider linear transmit precoding at the AP. At timeslot $t$ ($t = 0, \cdots, T$), the signal transmitted by the AP can be expressed as $\boldsymbol{u}^{(t)} = \boldsymbol{w}^{(t)} s^{(t)}$, where $s^{(t)}$ is the information symbol with a zero mean and unit variance (i.e., normalized power), $\boldsymbol{w}^{(t)} = \sqrt{P^{(t)}}\hat{\boldsymbol{w}}^{(t)}$ is the AP's beamforming vector at timeslot $t$, $\hat{\boldsymbol{w}}^{(t)} \in \mathbb{C}^{M\times 1}$ denotes the transmit beamforming direction vector, and $P^{(t)}$ is the transmit power of the AP at timeslot $t$. For given phase shifts $\boldsymbol{\Theta}_k^{(t)}$ of the $k$-th RIS at timeslot $t$, $k = 1, \cdots, K$, $\hat{\boldsymbol{w}}^{(t)}$ is given by [22]

$$\hat{\boldsymbol{w}}^{(t)} = \frac{\left(\boldsymbol{h}^{(t)}\right)^H}{\left\|\boldsymbol{h}^{(t)}\right\|}. \tag{12}$$

The signal received by the robot at timeslot $t$ is expressed as

$$y^{(t)} = \boldsymbol{h}^{(t)}\boldsymbol{w}^{(t)} s^{(t)} + n^{(t)}, \quad t = 0, \cdots, T, \tag{13}$$

where $n^{(t)} \sim \mathcal{CN}(0, \sigma^2)$ denotes the additive white Gaussian noise (AWGN) at the robot at timeslot $t$. Accordingly, the SNR received at the robot at timeslot $t$ is given by

$$SNR^{(t)} = \frac{\left|\boldsymbol{h}^{(t)}\boldsymbol{w}^{(t)}\right|^2}{\left|n^{(t)}\right|^2}, \quad t = 0, \cdots, T. \tag{14}$$

## III. Problem Formulation and Solution Algorithms

We formulate an optimization problem to minimize the total transmission energy consumption at the AP by jointly optimizing the number and locations of RISs, reflection-coefficients at RISs, and the beamforming vector at the AP, subject to a minimum received SNR constraint at the robot throughout its trajectory, i.e.,

$$(P1): \min_{K, q_{R_1}, \cdots, q_{R_K}, \boldsymbol{\Theta}_1^{(t)}, \cdots, \boldsymbol{\Theta}_K^{(t)}, \boldsymbol{w}^{(t)}} \sum_{t=0}^{T} \left\|\boldsymbol{w}^{(t)}\right\|^2 \tag{15}$$

$$s.t.\ C1: 0 \leqslant \theta_{k,n}^{(t)} < 2\pi,\ \forall k,\ \forall n,\ \forall t, \tag{15a}$$

$$C2: SNR^{(t)} \geqslant \gamma,\ \forall t, \tag{15b}$$

$$C3: K \geqslant 1, \tag{15c}$$

$$C4: 0 \leqslant P^{(t)} \leqslant P_{max},\ \forall t, \tag{15d}$$

$$C5: x_{R_k} = 0, y_{R_k} \in [0, l_f], z_{R_k} \in [z_r, h_{ce}],\ \forall k \tag{15e}$$

where $\gamma > 0$ is the minimum SNR requirement of the robot, $K$ is the number of RISs, $q_{Rk} = [x_{R_k}, y_{R_k}, z_{R_k}]$ is the position of the $k$-th RIS, $k = 1, \cdots, K$, $P_{max}$ is the maximum transmit power at the AP, and $h_{ce}$ is the height of the ceiling. The objective function $\sum_{t=0}^{T} \left\|\boldsymbol{w}^{(t)}\right\|^2$ is the total transmission energy consumption of the AP during the robot's journey. Constraint $C1$ imposes the value range of the phase shift for each element on the RISs, $C2$ ensures that the received SNR of the robot at each time slot is above the minimum SNR required, $C3$ ensures that at least one RIS will be deployed, $C4$ specifies the upper and lower bounds of the transmit power at the AP, and $C5$ is the constraint on the location of each RIS.

### A. TECO Algorithm

We note that it is hard to solve $(P1)$ directly due to the varying number of variables involved. We first study the case with the number $K$ and the locations of RISs fixed, for which $(P1)$ reduces to

$$(P2): \min_{\boldsymbol{\Theta}_1^{(t)}, \cdots, \boldsymbol{\Theta}_K^{(t)}, \boldsymbol{w}^{(t)}} \sum_{t=0}^{T} \left\|\boldsymbol{w}^{(t)}\right\|^2 \tag{16}$$
$$s.t.\ C1, C2, C4.$$

Since $\boldsymbol{w}^{(t)}$ and $\boldsymbol{\Theta}_k^{(t)}$ are independent for different $t$, the objective function of $(P2)$ is minimized when each $\left\|\boldsymbol{w}^{(t)}\right\|^2$ in the summation from $t = 0$ to $t = T$ is minimized. According to the above and substituting $\boldsymbol{w}^{(t)} = \sqrt{P^{(t)}}\hat{\boldsymbol{w}}^{(t)}$ into (16), $(P2)$ can be equivalently rewritten as

$$(P3): \min_{\boldsymbol{\Theta}_1^{(t)}, \cdots, \boldsymbol{\Theta}_K^{(t)}, P^{(t)}, \hat{\boldsymbol{w}}^{(t)}} P^{(t)} \left\|\hat{\boldsymbol{w}}^{(t)}\right\|^2,\ \forall t \in \{0, \cdots, T\} \tag{17}$$
$$s.t.\ C1, C2, C4.$$

Although $(P3)$ is still a non-convex problem and is difficult to solve directly, since $\left\|\hat{\boldsymbol{w}}^{(t)}\right\|^2 = 1$, we can obtain the optimal transmit power of the AP by substituting (14) into (15b) and solving the resulting inequality for $P^{(t)}$. Thus, the optimal transmit power of the AP is given by

$$P_{\text{opt}}^{(t)} = \frac{\gamma |n(t)|^2}{\left\|\left(\sum_{k=1}^{K} \boldsymbol{h}_{kR}^{(t)\,H} \boldsymbol{\Theta}_k^{(t)} \boldsymbol{G}_k^{(t)} + \boldsymbol{h}_{AR}^{(t)\,H}\right)\hat{\boldsymbol{w}}^{(t)}\right\|^2}. \tag{18}$$

By substituting (18) into $(P3)$ and assuming that the AP's maximum transmit power $P_{max}$ is sufficiently large (and hence $C4$ can be ignored for analytical tractability), we have

$$(P4): \min_{\boldsymbol{\Theta}_1^{(t)}, \cdots, \boldsymbol{\Theta}_K^{(t)}, \hat{\boldsymbol{w}}^{(t)}} \frac{\gamma |n(t)|^2}{\left\|\left(\sum_{k=1}^{K} \boldsymbol{h}_{kR}^{(t)\,H} \boldsymbol{\Theta}_k^{(t)} \boldsymbol{G}_k^{(t)} + \boldsymbol{h}_{AR}^{(t)\,H}\right)\hat{\boldsymbol{w}}^{(t)}\right\|^2}, \forall t \in \{0, \cdots, T\} \tag{19}$$
$$s.t.\ C1, C2.$$

Please note that $C4$ will be considered in our proposed Algorithm 2 (which will be presented later in this section) to ensure that the optimized transmit power of the AP does not go beyond its maximum allowed transmit power.

In order to solve $(P4)$, we divide it into two sub-problems $\hat{\boldsymbol{w}}^{(t)}$ and by fixing $\boldsymbol{\Theta}_k^{(t)}$ ($k = 1, \cdots, K, t = 0, \cdots, T$) in $(P4)$, respectively, as detailed below.

For a given $\hat{\boldsymbol{w}}^{(t)}$, $(P4)$ is equivalent to

$$(P5): \max_{\boldsymbol{\Theta}_1^{(t)}, \cdots, \boldsymbol{\Theta}_K^{(t)}} \left\|\left(\sum_{k=1}^{K} \boldsymbol{h}_{kR}^{(t)\,H} \boldsymbol{\Theta}_k^{(t)} \boldsymbol{G}_k^{(t)} + \boldsymbol{h}_{AR}^{(t)\,H}\right)\hat{\boldsymbol{w}}^{(t)}\right\|^2, \ \forall t \in \{0, \cdots, T\} \tag{20}$$

$$s.t.\ C1, C2$$

According to the triangle inequality, we have

$$\begin{aligned}&\left\|(\sum_{k=1}^{K}{\boldsymbol{h}_{kR}^{(t)}}^H\boldsymbol{\Theta}_k^{(t)}\boldsymbol{G}_k^{(t)}+{\boldsymbol{h}_{AR}^{(t)}}^H)\hat{\boldsymbol{w}}^{(t)}\right\|\\ \leqslant&\left\|{\boldsymbol{h}_{1R}^{(t)}}^H\boldsymbol{\Theta}_1^{(t)}\boldsymbol{G}_1^{(t)}\hat{\boldsymbol{w}}^{(t)}\right\|+\left\|{\boldsymbol{h}_{2R}^{(t)}}^H\boldsymbol{\Theta}_2^{(t)}\boldsymbol{G}_2^{(t)}\hat{\boldsymbol{w}}^{(t)}+,\cdots,\right.\\ &\left.+{\boldsymbol{h}_{KR}^{(t)}}^H\boldsymbol{\Theta}_K^{(t)}\boldsymbol{G}_K^{(t)}\hat{\boldsymbol{w}}^{(t)}+{\boldsymbol{h}_{AR}^{(t)}}^H\hat{\boldsymbol{w}}^{(t)}\right\|.\end{aligned}\tag{21}$$

The equality in (21) holds if and only if

$$\begin{aligned}&\arg({\boldsymbol{h}_{1R}^{(t)}}^H\boldsymbol{\Theta}_1^{(t)}\boldsymbol{G}_1^{(t)}\hat{\boldsymbol{w}}^{(t)})\\ =&\arg({\boldsymbol{h}_{2R}^{(t)}}^H\boldsymbol{\Theta}_2^{(t)}\boldsymbol{G}_2^{(t)}\hat{\boldsymbol{w}}^{(t)})+,\cdots,+\\ &\arg({\boldsymbol{h}_{KR}^{(t)}}^H\boldsymbol{\Theta}_K^{(t)}\boldsymbol{G}_K^{(t)}\hat{\boldsymbol{w}}^{(t)})+\arg({\boldsymbol{h}_{AR}^{(t)}}^H\hat{\boldsymbol{w}}^{(t)})\\ \triangleq&\Phi_1^{(t)},\end{aligned}\tag{22}$$

where $\arg(\boldsymbol{x})$ gives the phases of the elements of $\boldsymbol{x}$.

For given $\Theta_2^{(t)},\cdots,\Theta_K^{(t)}$ (and thus given $\Phi_1^{(t)}$), letting ${\boldsymbol{h}_{1R}^{(t)}}^H\boldsymbol{\Theta}_1^{(t)}\boldsymbol{G}_1^{(t)}\hat{\boldsymbol{w}}^{(t)}={\boldsymbol{\Theta}_1^{(t)}}^H\boldsymbol{R}_1^{(t)}$, where $\boldsymbol{R}_1^{(t)}=diag({\boldsymbol{h}_{1R}^{(t)}}^H)\boldsymbol{G}_1^{(t)}\hat{\boldsymbol{w}}^{(t)}$, and substituting (21) under the condition of (22) into $(P5)$, we have

$$(P6):\ \max_{\boldsymbol{\Theta}_1^{(t)}}\left\|{\boldsymbol{\Theta}_1^{(t)}}^H\boldsymbol{R}_1^{(t)}\right\|^2,\ \forall t\in\{0,\cdots,T\}\tag{23}$$

$$s.t.\qquad C1$$

$$C6:\arg({\boldsymbol{\Theta}_1^{(t)}}^H\boldsymbol{R}_1^{(t)})=\Phi_1^{(t)}.\tag{23a}$$

According to (22), we can show that the optimal solution to $(P6)$ is given by

$$\boldsymbol{\Theta}_{1\text{opt}}^{(t)}=e^{j(\Phi_1^{(t)}-\arg(\boldsymbol{R}_1^{(t)}))},\tag{24}$$

which suggests that the phase shifts of $\text{RIS}_1$ should be tuned according to the beamforming of the AP and the phase shifts of $\text{RIS}_k$, $k=2,\cdots,K$.

Following the similar procedures as above, the optimal phase shifts of $\text{RIS}_k(k=2,\cdots,K)$ can be obtained as

$$\boldsymbol{\Theta}_{k\text{opt}}^{(t)}=e^{j(\Phi_k^{(t)}-\arg(\boldsymbol{R}_k^{(t)}))},\tag{25}$$

where $\boldsymbol{R}_k^{(t)}=diag({\boldsymbol{h}_{kR}^{(t)}}^H)\boldsymbol{G}_k^{(t)}\hat{\boldsymbol{w}}^{(t)}$ and $\Phi_k^{(t)}$ is given by

$$\begin{aligned}&\Phi_k^{(t)}\\ \triangleq&\arg({\boldsymbol{h}_{1R}^{(t)}}^H\boldsymbol{\Theta}_1^{(t)}\boldsymbol{G}_1^{(t)}\hat{\boldsymbol{w}}^{(t)})+,\cdots,+\\ &\arg({\boldsymbol{h}_{(k-1)R}^{(t)}}^H\boldsymbol{\Theta}_{k-1}^{(t)}\boldsymbol{G}_{k-1}^{(t)}\hat{\boldsymbol{w}}^{(t)})\\ &+\arg({\boldsymbol{h}_{(k+1)R}^{(t)}}^H\boldsymbol{\Theta}_{k+1}^{(t)}\boldsymbol{G}_{k+1}^{(t)}\hat{\boldsymbol{w}}^{(t)})+,\cdots,+\\ &\arg({\boldsymbol{h}_{KR}^{(t)}}^H\boldsymbol{\Theta}_K^{(t)}\boldsymbol{G}_K^{(t)}\hat{\boldsymbol{w}}^{(t)})+\arg({\boldsymbol{h}_{AR}^{(t)}}^H\hat{\boldsymbol{w}}^{(t)})\end{aligned}\tag{26}$$

For given $\boldsymbol{\Theta}_k^{(t)},k=1,\cdots,K,t\in\{0,\cdots,T\}$, $(P4)$ converts to

$$\begin{aligned}(P7):\max_{\hat{\boldsymbol{w}}^{(t)}}&\left\|(\sum_{k=1}^{K}{\boldsymbol{h}_{kR}^{(t)}}^H\boldsymbol{\Theta}_k^{(t)}\boldsymbol{G}_k^{(t)}+{\boldsymbol{h}_{AR}^{(t)}}^H)\hat{\boldsymbol{w}}^{(t)}\right\|^2\\ &,\ \forall t\in\{0,\cdots,T\}\end{aligned}\tag{27}$$

$$s.t.\quad C2$$

Based on (14) and (15b), we solve $(P7)$ and obtain the optimal transmit beamforming direction vector $\hat{\boldsymbol{w}}_{\text{opt}}^{(t)}$ of the AP as [22]

$$\hat{\boldsymbol{w}}_{\text{opt}}^{(t)}=\frac{\left(\sum_{k=1}^{K}{\boldsymbol{h}_{kR}^{(t)}}^H\boldsymbol{\Theta}_k^{(t)}\boldsymbol{G}_k^{(t)}+{\boldsymbol{h}_{AR}^{(t)}}^H\right)^H}{\left\|\sum_{k=1}^{K}{\boldsymbol{h}_{kR}^{(t)}}^H\boldsymbol{\Theta}_k^{(t)}\boldsymbol{G}_k^{(t)}+{\boldsymbol{h}_{AR}^{(t)}}^H\right\|}.\tag{28}$$

We can obtain the optimal transmit power $P_{\text{opt}}^{(t)}$ of the AP by substituting (24), (25), and (28) into (18).

Based on the above solutions to the two subproblems $(P5)$ and $(P7)$, we propose an iterative algorithm that solves $(P5)$ and $(P7)$ alternately in each iteration to minimize the total energy consumption at the AP, i.e., the TECO algorithm as presented in Algorithm 2. In each iteration, according to (21) and (22), calculating (24) or (25) guarantees that the objective function of (P5) is non-decreasing, and calculating (28) guarantees that the objective function of (P7) is non-decreasing [22]. As a result, after each iteration, the objective function value of (P4) is non-increasing. Since there is a lower bound of the objective function of $(P4)$ given by $C2$, the objective function of $(P4)$ will decrease after each iteration until its convergence. In Algorithm 2, solving $(P5)$ has a complexity of $\mathcal{O}(\frac{N}{K}\times K)=\mathcal{O}(N)$, where $N$ is the total number of passive reflecting elements of all the RISs, while

**Algorithm 2** TECO Algorithm

**Input:** $\boldsymbol{h}_{kR}^{(t)},\boldsymbol{G}_k^{(t)},\boldsymbol{h}_{AR}^{(t)},\boldsymbol{q}_R$
**Output:** $\hat{\boldsymbol{w}}_{\text{opt}}^{(t)},\boldsymbol{\Theta}_{k\text{opt}}^{(t)},P_{\text{opt}}^{(t)}$

1: Set the iteration index $s=1$ and initialize the AP's transmit beamforming direction $\hat{\boldsymbol{w}}_{\text{opt}(s)}^{(t)}$.
2: Initialize the RIS phase shifts $\boldsymbol{\Theta}_{k(s)}^{(t)}$, $k=1,\cdots,K$.
3: Obtain $P_{\text{opt}(s)}^{(t)}$ according to (18).
4: **repeat**
5: Update $s=s+1$.
6: Obtain $\boldsymbol{\Theta}_{k(s)}^{(t)}$, $k=1,\cdots,K$, using (24) or (25).
7: Obtain $\hat{\boldsymbol{w}}_{\text{opt}(s)}^{(t)}$ according to (28).
8: Obtain $P_{\text{opt}(s)}^{(t)}$ according to (18).
9: $P_{\text{opt}(s)}^{(t)}=min\left\{P_{\text{opt}(s)}^{(t)},P_{max}\right\}$
10: **until** $P_{\text{opt}(s-1)}^{(t)}-P_{\text{opt}(s)}^{(t)}<\varepsilon$.
11: $\hat{\boldsymbol{w}}_{\text{opt}}^{(t)}=\hat{\boldsymbol{w}}_{\text{opt}(s)}^{(t)}$, $\boldsymbol{\Theta}_{k\text{opt}}^{(t)}=\boldsymbol{\Theta}_{k(s)}^{(t)}$, $P_{\text{opt}}^{(t)}=P_{\text{opt}(s)}^{(t)}$,$k=1,\cdots,K$.

solving $(P7)$ has a complexity of $\mathcal{O}(M)$, where $M$ is the number of antennas at the AP. Thus, Algorithm 2 has a complexity of $\mathcal{O}(N_I(M+N))$, where $N_I$ is the number of iterations required for convergence.

### *B. RISLN Algorithm*

In order to optimize the number and locations of RISs, we divide the wall area where the RISs are deployed into a grid of $\lceil \frac{l_f \times (l_h - z_r)}{d_u^2} \rceil$ equal rectangular units, where $l_f$ is the length of the wall, $l_h$ is the height of the wall, $z_r$ is the height of the robot antenna, and $d_u^2$ is approximately the size of each RIS. We assume that each RIS is deployed in one of the units and no more than one RIS can be deployed in any unit. Hence, the location of the $k$-th RIS, $q_{Rk}, \forall k \in \{1, \cdots, K\}$, can be uniquely represented by a sequence of $b = \lceil \log_2(\frac{l_f \times (l_h - z_r)}{d_u^2}) \rceil$ binary bits.

Given $I$ obstacles in the considered indoor environment, we can show that there is no need to deploy more than $I+1$ RISs to ensure the robot seeing a LoS link from at least one RIS or the AP at all times along its trajectroy. For each $K \in \{1, \cdots, I+1\}$, we employ Algorithm 2 and the Genetic Algorithm [23] to optimize the locations of the $K$ RISs as follows. First, set the iteration index $s' = 1$, and randomly initialize a population of $N_{\text{ind}}$ individuals, where $N_{\text{ind}}$ is an even number and each individual contains a binary bit sequence $\boldsymbol{q}_R = [q_{R_1}, q_{R_2}, \cdots, q_{R_K}]$ that represents the locations of $K$ RISs. Then, Algorithm 2 is used to obtain $\hat{\boldsymbol{w}}_{\text{opt}}^{(t)}, \boldsymbol{\Theta}_{\text{kopt}}^{(t)}, P_{\text{opt}}^{(t)}$, $t \in \{0, \cdots, T\}$, $k \in \{1, \cdots, K\}$ for each individual and $\sum_{t=0}^{T} P_{\text{opt}}^{(t)}$ is taken as the fitness value of the corresponding individual.

Update $s' = s'+1$, and a new population of $N_{\text{ind}}$ individuals are generated from the current population by the Roulette Wheel Selection scheme [23], where each individual has a probability of selection proportional to its fitness value. Next, the population generated by Selection is randomly divided into $\frac{N_{\text{ind}}}{2}$ pairs of individuals. For each pair, generate a random number $r$ following a uniform distribution in $(0, 1)$ and swap the $\lfloor (Kb/2) \rfloor$-th to the $Kb$-th bits between the two individuals if $r \leqslant \mathcal{P}_c$, where $0 < \mathcal{P}_c < 1$ is the Crossover probability. Afterwards, for each individual in the new population generated by Crossover, generate a random number $r'$ following a uniform distribution in $(0, 1)$ and flip every binary bit of the corresponding individual if $r' \leqslant \mathcal{P}_m$, where $0 < \mathcal{P}_m < 1$ is the Mutation probability. Then, for each individual in the new population generated by Mutation, Algorithm 2 is used to obtain $\hat{\boldsymbol{w}}_{\text{opt}}^{(t)}, \boldsymbol{\Theta}_{\text{kopt}}^{(t)}$ and $P_{\text{opt}}^{(t)}$, $t \in \{0, \cdots, T\}, k \in \{1, \cdots, K\}$. The individual that has the smallest fitness value among the population is identified, and its $\hat{\boldsymbol{w}}_{\text{opt}}^{(t)}, \boldsymbol{\Theta}_{\text{kopt}}^{(t)}$ and $P_{\text{opt}}^{(t)}$ are labeled as $\hat{\boldsymbol{w}}_{\text{opt}K(s')}^{(t)}, \boldsymbol{\Theta}_{\text{kopt}K(s')}^{(t)}$ and $P_{\text{opt}K(s')}^{(t)}$, $t \in \{0, \cdots, T\}, k \in \{1, \cdots, K\}$, respectively.

The above Selection, Crossover and Mutation procedures repeat until $\sum_{t=0}^{T} P_{\text{opt}K(s'-1)}^{(t)} - \sum_{t=0}^{T} P_{\text{opt}K(s')}^{(t)} < \varepsilon$, where $\varepsilon$ is a positive constant. Once converged, the individual that has the smallest fitness value among the latest population is identified as the optimal locations of $K$ RISs, labeled as $\boldsymbol{q}_{R\text{opt}K}$, and its $\hat{\boldsymbol{w}}_{\text{opt}K(s')}^{(t)}, \boldsymbol{\Theta}_{\text{kopt}K(s')}^{(t)}$ and $P_{\text{opt}K(s')}^{(t)}$ are labeled as $\hat{\boldsymbol{w}}_{\text{opt}K}^{(t)}, \boldsymbol{\Theta}_{\text{kopt}K}^{(t)}$ and $P_{\text{opt}K}^{(t)}$, $t \in \{0, \cdots, T\}, k \in \{1, \cdots, K\}$, respectively. The above iterative algorithm for each $K$ is ensured to converge when the iteration number is large enough [23].

After the optimized locations of $K$ RISs have been obtained for all $K \in \{1, \cdots, I+1\}$, the value of $K$ that is associated with the lowest value of $\sum_{t=0}^{T} P_{\text{opt}K}^{(t)}$ is identified as the optimal value of $K$ and its corresponding $q_{R\text{opt}K}$, $\sqrt{P_{\text{opt}K}^{(t)}} \hat{\boldsymbol{w}}_{\text{opt}K}^{(t)}$ and $\boldsymbol{\Theta}_{\text{kopt}K}^{(t)}$, $t \in \{0, \cdots, T\}$, $k \in \{1, \cdots, K\}$ return the optimal RIS locations, AP beamforming vectors and RIS phase shifts, respectively.

The above described RIS Locations and Number (RISLN) Algorithm is presented in Algorithm 3. It has a complexity of $\mathcal{O}((T+1)N_I(M+N)N_{\text{ind}} \sum_{K=1}^{I+1} N_{GK})$, where $N_{GK}$ is the number of iterations required for $K \in \{1, \cdots, I+1\}$.

TABLE I
PARAMETER VALUES USED IN THE SIMULATION

| Parameter | | Value |
|---|---|---|
| $l_f$ | length of the wall where RISs are deployed | $18m$ |
| $l_p$ | length of the wall parallel to obstacle's rows | $20m$ |
| $l_h$ | height of the wall where RISs are deployed | $12m$ |
| $I$ | number of obstacles | 3 |
| $q_{O_1}$ | location of Obstacle 1 | $[19, 1, 0]m$ |
| $q_{O_2}$ | location of Obstacle 2 | $[19, 8, 0]m$ |
| $q_{O_3}$ | location of Obstacle 3 | $[19, 15, 0]m$ |
| $L$ | length of each obstacle | $15m$ |
| $W$ | width of each obstacle | $2m$ |
| $H$ | height of each obstacle | $10m$ |
| $l_a$ | distance between two adjacent obstacles | $5m$ |
| $l$ | distance between robot and obstacle | $1m$ |
| $q_s$ | robot's start point | $[19, 0, 0]m$ |
| $q_d$ | robot's destination point | $[19, 18, 0]m$ |
| $z_r$ | height of the robot antenna | $1m$ |
| $v_t$ | speed of the robot | $1m/s$ |
| $q_A$ | location of the AP | $[1, 6, 12]m$ |
| $d$ | AP's spacing between adjacent antennas | $\lambda/2$ |
| $M$ | number of antennas on the AP | 5 |
| $N$ | total number of elements on all RISs | 90 |
| $d_u^2$ | approximate RIS size used in Algorithm 3 | $1cm^2$ |
| $\beta_{AR} = \beta_{kR}$ | path loss exponent [25] | 4 |
| $\rho$ | LoS path gain [21] | $-30dB$ |
| $\sigma^2$ | noise power [21] | $-109dBm$ |
| $\gamma$ | minimum SNR requirement | $10dB$ |
| $f_c$ | carrier frequency | $60GHz$ |
| $\mathcal{P}_c$ | crossover probability | 0.6 |
| $\mathcal{P}_m$ | mutation probability | 0.01 |
| $N_{\text{ind}}$ | number of individuals in a population | 20 |
| $\varepsilon$ | convergence threshold | 0.001 |

## IV. SIMULATION RESULTS

In this section, we present numerical results to verify the proposed algorithms. The parameter values used in the simulation are listed in Table I unless otherwise specified.

Fig. 2 shows the transmission energy consumption of the AP versus the iteration number in Algorithm 3. The fluctuation

**Algorithm 3** RISLN Algorithm

**Input:** $\mathcal{P}_c, \mathcal{P}_m, N_{\text{ind}}, I$ $(0 < I \leqslant l_f/(l_a + W))$.

**Output:** $K_{\text{opt}}$, $q_{R\text{opt}K}$, $\sqrt{P^{(t)}_{\text{opt}K}}\hat{\boldsymbol{w}}^{(t)}_{\text{opt}K}$, $\boldsymbol{\Theta}^{(t)}_{\text{kopt}K}$, $t \in \{0, \cdots, T\}$, $k \in \{1, \cdots, K\}$.

Initialize the number of RISs $K = 1$.
**repeat**
  Set the iteration index $s' = 1$, and randomly initialize a population of $N_{\text{ind}}$ individuals, where each individual is a binary bit sequence $\boldsymbol{q}_R = [q_{R_1}, q_{R_2}, \cdots, q_{R_K}]$. Run Algorithm 2 for $t = 0, \cdots, T$ for each individual and take $\sum_{t=0}^{T} P^{(t)}_{\text{opt}}$ as its fitness value.
  **repeat**
    Update $s' = s' + 1$
    Selection: Obtain a new population of $N_{\text{ind}}$ individuals from the current population by the Roulette Wheel Selection scheme [23].
    Crossover: The new population is randomly divided into $\frac{N_{\text{ind}}}{2}$ pairs. For each pair, randomly generate $r \in (0, 1)$ and swap the $\lfloor (Kb/2) \rfloor$-th to the $Kb$-th bits between the two individuals if $r \leqslant \mathcal{P}_c$.
    Mutation: For each individual in the population generated by Crossover, randomly generate $r' \in (0, 1)$ and flip every bit of it if $r' \leqslant \mathcal{P}_m$.
    Run Algorithm 2 for each individual in the population generated by Mutation. The individual that has the smallest fitness value returns $\hat{\boldsymbol{w}}^{(t)}_{\text{opt}K(s')}$, $\boldsymbol{\Theta}^{(t)}_{\text{kopt}K(s')}$ and $P^{(t)}_{\text{opt}K(s')}$, $t \in \{0, \cdots, T\}$, $k \in \{1, \cdots, K\}$.
  **until** $\sum_{t=0}^{T} P^{(t)}_{\text{opt}K(s'-1)} - \sum_{t=0}^{T} P^{(t)}_{\text{opt}K(s')} < \varepsilon$.
  $P^{(t)}_{\text{opt}K} = P^{(t)}_{\text{opt}K(s')}$, $\hat{\boldsymbol{w}}^{(t)}_{\text{opt}K} = \hat{\boldsymbol{w}}^{(t)}_{\text{opt}K(s')}$, $\boldsymbol{\Theta}^{(t)}_{\text{kopt}K} = \boldsymbol{\Theta}^{(t)}_{\text{kopt}K(s')}$, $t \in \{0, \cdots, T\}$, $k \in \{1, \cdots, K\}$.
  Update $K = K + 1$.
**until** $K = I + 2$.
$K_{opt} = \underset{K\{1,\cdots,I+1\}}{\arg\min} \left\{ \sum_{t=0}^{T} P^{(t)}_{\text{opt}K} \right\}$ and return its $q_{R\text{opt}K}$, $\sqrt{P^{(t)}_{\text{opt}K}}\hat{\boldsymbol{w}}^{(t)}_{\text{opt}K}$, $\boldsymbol{\Theta}^{(t)}_{\text{kopt}K}$, $t \in \{0, \cdots, T\}$, $k \in \{1, \cdots, K\}$ as output.

of the curve is due to the use of the Genetic Algorithm that randomly generates a new population of candidate solutions in each iteration. By generating new populations, the genetic algorithm introduces genetic diversity so as to escape local optima by exploring different regions of the solution space, but the AP's transmission energy consumption of a randomly generated new population is not necessarily lower than that of the population obtained in the previous iteration. We can see that Algorithm 3 converges after the 19th iteration.

In the simulation, we compare the performance of Algorithm 3 with the following four benchmark schemes: the evenly distributed RIS deployment scheme proposed in [24],

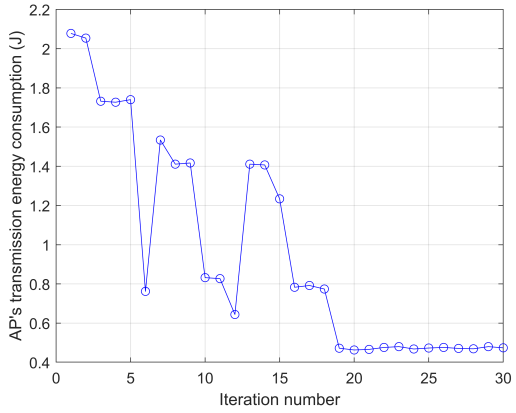


Fig. 2. Transmission energy consumption of the AP versus the iteration number.

where the RISs are evenly spaced on the wall at the same height, and the number and the height of RISs are the optimal results obtained by Algorithm 3; the centralized deployment (i.e., a single RIS) with the optimal location of the RIS obtained by Algorithm 3 for $K = 1$; the centralized deployment of one RIS at the centre of the wall; and the case without deploying any RIS. For all the RIS deployment schemes under comparison, the RISs are deployed on the same wall as shown in Fig. 1. The specific locations of RISs for the four RIS deployment schemes are indicated in Fig. 3.

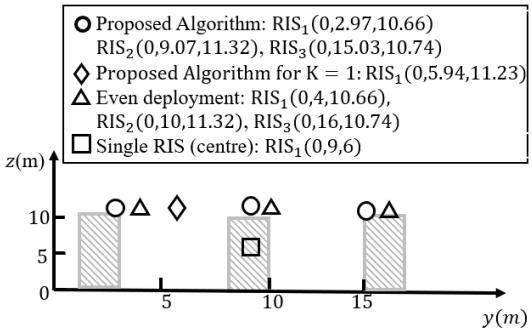


Fig. 3. Locations of RISs.

Fig. 4 plots the AP's transmission energy consumption versus the minimum required SNR at the robot. The optimal number of RISs obtained by the proposed algorithm is $K_{opt} = 3$. As shown in Fig. 4, the transmission energy consumption at the AP increases when the minimum required SNR at the robot increases, since a higher target SNR at the robot requires higher transmit power at the AP at each timeslot. The optimal RIS deployment obtained by Algorithm 3 achieves the lowest energy consumption at the AP among all the considered schemes. Compared with the evenly distributed RIS deployment scheme, deploying a single RIS at the optimal location obtained by Algorithm 3 for $K = 1$ leads to a lower energy consumption at the AP. This is because Algorithm 3 optimizes the RIS location while considering the

exact locations of obstacles and the robot. Between the two schemes both without optimizing the RIS location, the evenly distributed deployment outperforms deploying a single RIS at the center of the wall because the multiple distributed RISs make it more likely for the robot to see a LoS link from one of the RISs along the whole trajectory than a single RIS. The case with no RIS always has the highest transmission energy consumption at the AP among all the considered schemes. This indicates that the deployment of RIS can decrease the transmission energy consumption at the AP.

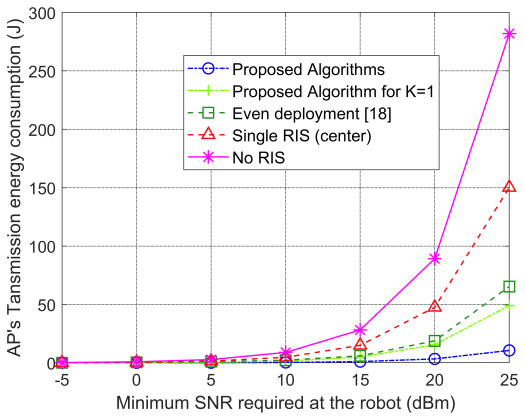


Fig. 4. AP's transmission energy consumption versus the minimum required SNR at the robot.

In Fig. 5, we plot the transmission energy consumption at the AP versus the total number of elements on RISs. The optimal number of RISs obtained by the proposed algorithm is $K_{opt} = 3$. In addition to the four benchmark shcemes considered in Fig. 4, we also plot a curve for the even deployment scheme [24] with $K = 2K_{opt}$. The AP's transmission energy consumption decreases with the total number of elements on RISs under all the considered schemes, because a larger number of elements leads to a larger beamforming gain of the RISs. The proposed algorithm performs the best because the optimized deployment locations of RISs ensure that the robot sees a LoS link from an RIS or the AP throughout its trajectory and the AP can transmit at the lowest possible power at each timeslot. The even deployment scheme for $K = K_{opt}$ achieves a lower transmission energy consumption of the AP than the even deployment scheme for $K = 2K_{opt}$. This indicates that further distributing the fixed total number of elements to more RISs cannot further lower the AP's transmission energy consumption if the whole trajectory has already been covered with LoS links, while less elements per RIS will reduce the beamforming gain of each RIS.

In Fig. 6, we plot the transmission energy consumption at the AP versus the carrier frequency of the mmWave signal. The optimal number of RISs obtained by the proposed algorithm is $K_{opt} = 3$. For all the considered schemes, the transmission energy consumption at the AP increases with the carrier frequency of the signal because the signal strength decays faster over distance at a higher carrier frequency. The performance gain of the proposed algorithm over the other schemes becomes larger with the increase of the carrier frequency. This shows the importance of optimizing RIS deployment for indoor downlink transmissions in high mmWave bands.

In Fig. 7, we plot the transmission energy consumption at the AP versus the number of obstacles. The transmission energy consumption at the AP increases with the number of obstacles for all the considered schemes because of the robot's longer trajectory. The proposed algorithm, the proposed algorithm for $K = 1$ and the even deployment scheme have the same AP's transmission energy consumption when the number of obstacle is one, because deploying one RIS is enough for the robot to maintain a LoS link from the RIS or the AP along the whole trajectory. The even deployment scheme outperforms the proposed algorithm for $K = 1$ when the number of obstacles is four or five, because the centralized deployment scheme keeps the robot seeing a LoS link from the RIS or the AP for fewer timeslots.

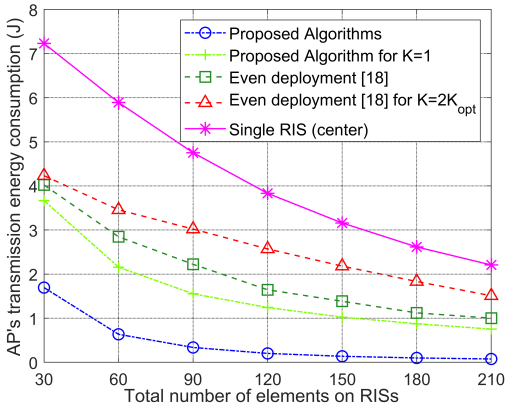


Fig. 5. AP's transmission energy consumption versus the total number of elements on RISs.

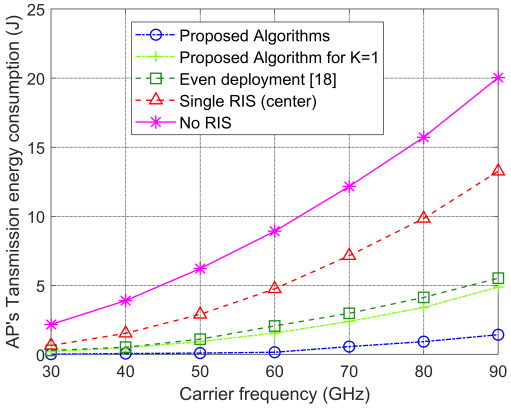


Fig. 6. AP's transmission energy consumption versus the carrier frequency of the signal.

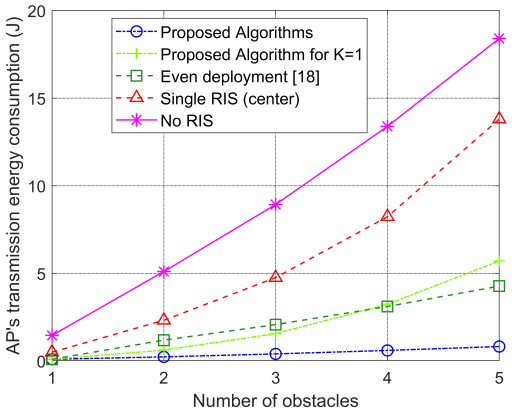


Fig. 7. AP's transmission energy consumption versus the number of obstacles.

## V. Conclusion and Future Work

In this paper, we have studied multiple-RIS-assisted mmWave communications for a robot moving around obstacles along a predefined trajectory inside an industrial building. To minimize the transmission energy consumption at the AP while ensuring the received SNR at the robot above a threshold throughout its journey, we have proposed the TECO Algorithm and RISLN Algorithm that jointly optimize the number, locations and phase shifts of RISs and the beamforming vector of the AP. Simulation results demonstrate that the proposed algorithms converge fast and can significantly reduce the transmission energy consumption at the AP as compared to the benchmark schemes that either do not deploy any RIS or do not optimize the number or locations of RISs. Distributing the fixed total number of reflecting elements to more RISs leads to a lower transmission energy consumption of the AP, since more distributed RISs provide more LoS links to the robot while it moves along its trajectory. The reduction in AP transmission energy consumption stops when the number of RISs becomes too large. This is because when all sections of the robot trajectory have been covered by LoS links from either the AP or an RIS, further dividing the fixed total number of reflecting elements into more RISs will reduce the beamforming gain of each RIS. For the considered scenario of $I$ obstacles, properly deploying $I$ RISs is sufficient to ensure that the robot sees a LoS link from at least one RIS or the AP at all times along its trajectory. The AP's transmission energy consumption increases with the minimum SNR required at the robot and the carrier frequency of the mmWave signal, but decreases with a larger total number of elements on the RISs.

In our future work, we will study the AP transmission energy consumption minimization problem where the robot's trajectory can be jointly optimized with the deployment of the AP and RISs. We will also extend out work to more complex scenarios, e.g., multiple robots moving along different trajectories. This will require allocating the available RISs and AP beamforming vectors to different robots while considering potential co-channel interference among the links serving neighboring robots. It will also be interesting to consider the energy consumption of RISs when the reflecting elements are not fully passive.

## References


[1] S. Haddadin, A. De Luca and A. Albu-Schäffer, "Robot collisions: A survey on detection, isolation, and identification," in IEEE Transactions on Robotics, vol. 33, no. 6, pp. 1292-1312, Dec. 2017.

[2] T. S. Rappaport, G. R. MacCartney, M. K. Samimi and S. Sun, "Wideband millimeter-wave propagation measurements and channel models for future wireless communication system design," in IEEE Transactions on Communications, vol. 63, no. 9, pp. 3029-3056, Sept. 2015.

[3] A. N. Uwaechia and N. M. Mahyuddin, "A comprehensive survey on millimeter wave communications for fifth-generation wireless networks: Feasibility and challenges," in IEEE Access, vol. 8, pp. 62367-62414, 2020.

[4] M. Di Renzo, M. Debbah, D.-T. Phan-Huy, A. Zappone, M.-S. Alouini, C. Yuen, et al., "Smart radio environments empowered by reconfigurable AI meta-surfaces: An idea whose time has come", EURASIP J. Wireless Commun. Netw., vol. 2019, pp. 129, May 2019.

[5] Q. Wu and R. Zhang, "Towards smart and reconfigurable environment: Intelligent reflecting surface aided wireless network," in IEEE Communications Magazine, vol. 58, no. 1, pp. 106-112, January 2020.

[6] Q. Wu and R. Zhang, "Intelligent reflecting surface enhanced wireless network via joint active and passive beamforming," in IEEE Transactions on Wireless Communications, vol. 18, no. 11, pp. 5394-5409, Nov. 2019.

[7] H. Du, J. Zhang, J. Cheng, and B. Ai, "Millimeter wave communications with reconfigurable intelligent surfaces: Performance analysis and optimization," IEEE Trans. Commun., vol. 69, no. 4, pp. 2752–2768, Apr. 2021.

[8] S. Lin, B. Zheng, G. C. Alexandropoulos, M. Wen, M. D. Renzo and F. Chen, "Reconfigurable intelligent surfaces with reflection pattern modulation: Beamforming design and performance analysis," in IEEE Transactions on Wireless Communications, vol. 20, no. 2, pp. 741-754, Feb. 2021.

[9] J. Lyu and R. Zhang, "Spatial throughput characterization for intelligent reflecting surface aided multiuser system," in IEEE Wireless Communications Letters, vol. 9, no. 6, pp. 834-838, June 2020.

[10] S. Zhang and R. Zhang, "Intelligent reflecting surface aided multiple access: Capacity region and deployment strategy," 2020 IEEE 21st International Workshop on Signal Processing Advances in Wireless Communications (SPAWC), Atlanta, GA, USA, 2020, pp. 1-5.

[11] Y. Han, S. Zhang, L. Duan and R. Zhang, "Cooperative double-IRS aided communication: Beamforming design and power scaling," in IEEE Wireless Communications Letters, vol. 9, no. 8, pp. 1206-1210, Aug. 2020.

[12] Y. Zhang, J. Zhang, M. Di Renzo, H. Xiao and B. Ai, "Reconfigurable intelligent surfaces with outdated channel state information: Centralized vs. distributed deployments," in IEEE Transactions on Communications, vol. 70, no. 4, pp. 2742-2756, Apr. 2022.

[13] S. Pala, K. Singh, M. Katwe and C. -P. Li, "Joint optimization of URLLC parameters and beamforming design for multi-RIS-aided MU-MISO URLLC system," in IEEE Wireless Communications Letters, vol. 12, no. 1, pp. 148-152, Jan. 2023.

[14] K. Zhao, H. Mei, S. Lyu and L. Peng, "Joint optimization of multiple UAV-mounted RISs deployment and RIS elements allocation," 2022 13th International Conference on Information and Communication Technology Convergence (ICTC), Jeju Island, Korea, Republic of, 2022, pp. 1193-1197.

[15] C. Tatino, N. Pappas and D. Yuan, "Robot trajectory planning with QoS constrained IRS-assisted millimeter-wave communications," IEEE International Conference on Communications, 2021, pp. 1-6.

[16] M. Eskandari, H. Huang, A. V. Savkin and W. Ni, "Model predictive control-based 3D navigation of a RIS-equipped UAV for LoS wireless communication with a ground intelligent vehicle," in IEEE Transactions on Intelligent Vehicles, 2022.

[17] N. Agrawal, A. Bansal, K. Singh and C. -P. Li, "Performance evaluation of RIS-assisted UAV-enabled vehicular communication system with multiple non-identical interferers," in IEEE Transactions on Intelligent Transportation Systems, vol. 23, no. 7, pp. 9883-9894, July 2022.

[18] Y. Yu, X. Liu and V. C. M. Leung, "Fair downlink communications for RIS-UAV enabled mobile vehicles," in IEEE Wireless Communications Letters, vol. 11, no. 5, pp. 1042-1046, May 2022.

[19] A. Bansal, N. Agrawal, and K. Singh, “Rate-splitting multiple access for UAV-based RIS-enabled interference-limited vehicular communication system,” IEEE Trans. Intel. Veh., 2022.
[20] E. Martin, M. Marcus, G. Thorsten and M. Stefan,”Fast ray/axis-aligned bounding box overlap tests using ray slopes,” Journal of Graphics Tools, vol. 12, no. 4, pp. 35-46, 2007.
[21] J. He, H. Wymeersch, T. Sanguanpuak, O. Silven and M. Juntti,” Adaptive beamforming design for mmWave RIS-aided joint localization and communication,” 2020 IEEE Wireless Communications and Networking Conference Workshops (WCNCW), 2020, pp. 1-6.
[22] T. K. Y. Lo, ”Maximum ratio transmission,” in IEEE Transactions on Communications, vol. 47, no. 10, pp. 1458-1461, Oct. 1999.
[23] R. L. Haupt and D. H. Werner,”Appendix: MATLAB code,” in Genetic Algorithms in Electromagnetics, IEEE, 2007, pp.269-275.
[24] Z. Li, H. Hu, J. Zhang and J. Zhang, ”Coverage analysis of multiple transmissive RIS-aided outdoor-to-indoor mmWave networks,” in IEEE Transactions on Broadcasting, vol. 68, no. 4, pp. 935-942, Dec. 2022.
[25] V. Dharmadhikari, N. Pusalkar and P. Ghare, ”Path loss exponent estimation for wireless sensor node positioning: Practical approach,” 2018 IEEE International Conference on Advanced Networks and Telecommunications Systems (ANTS), 2018, pp. 1-4.